nature physics

ARTICLES

https://doi.org/10.1038/s41567-020-0903-z

Check for updates

High-fidelity entanglement and detection of alkaline-earth Rydberg atoms

Ivaylo S. Madjarov[1,4], Jacob P. Covey[1,4], Adam L. Shaw[1], Joonhee Choi[1], Anant Kale[1], Alexandre Cooper[1,3], Hannes Pichler[1], Vladimir Schkolnik[2], Jason R. Williams[2] and Manuel Endres[1]✉

Trapped neutral atoms have become a prominent platform for quantum science, where entanglement fidelity records have been set using highly excited Rydberg states. However, controlled two-qubit entanglement generation has so far been limited to alkali species, leaving the exploitation of more complex electronic structures as an open frontier that could lead to improved fidelities and fundamentally different applications such as quantum-enhanced optical clocks. Here, we demonstrate a novel approach utilizing the two-valence electron structure of individual alkaline-earth Rydberg atoms. We find fidelities for Rydberg state detection, single-atom Rabi operations and two-atom entanglement that surpass previously published values. Our results pave the way for novel applications, including programmable quantum metrology and hybrid atom–ion systems, and set the stage for alkaline-earth based quantum computing architectures.

Recent years have seen remarkable advances in generating strong, coherent interactions in arrays of neutral atoms through excitation to Rydberg states, characterized by large electronic orbits[1–4]. This has led to profound results in quantum science applications, such as quantum simulation[4–7] and quantum computing[2,3,8–11], including a record for two-atom entanglement for neutral atoms[9]. Furthermore, up to 20 qubit entangled states have been generated in Rydberg arrays[12], which is competitive with results in trapped ions[13] and superconducting circuits[14]. Many of these developments have been fueled by novel techniques for generating reconfigurable atomic arrays[15–17] and mitigation of noise sources[9,18]. Although previous Rydberg-atom-array experiments have utilized alkali species, atoms with a more complex level structure, such as the alkaline-earth atoms (AEAs)[19–24] commonly used in optical lattice clocks[25], provide new opportunities for increasing fidelities and accessing fundamentally different applications, including Rydberg-based quantum metrology[26–28], quantum clock networks[29] and quantum computing schemes with optical and nuclear qubits[30,31].

Here, we demonstrate such a novel Rydberg array architecture based on AEAs, where we utilize the two-valence electron structure for single-photon Rydberg excitation from a metastable clock state as well as auto-ionization detection of Rydberg atoms (Fig. 1). We find leading fidelities for Rydberg state detection, ground-to-Rydberg-state coherent operations and Rydberg-based two-atom entanglement (Table 1). More generally, our results demonstrate the highest-reported two-atom entanglement fidelities for neutral atoms[9,32,33] as well as a proof of principle for controlled two-atom entanglement between AEAs. We further demonstrate a high-fidelity entanglement operation with optical traps kept on, an important step for gate-based quantum computing[1–3,8–11]. As detailed in the following, our results open up a host of new opportunities for quantum metrology and computing as well as for optical trapping of ions.

Our experimental system[23,34,35] combines various novel key elements. First, we implement atom-by-atom assembly in reconfigurable tweezer arrays[15,16] for AEAs (Fig. 1b). Second, we sidestep the typical protocol for two-photon excitation to S-series Rydberg states, which requires significantly higher laser power to suppress intermediate state scattering by transferring atoms to the long-lived $^3P_0$ clock state $|g\rangle$[25,34–36]. We treat $|g\rangle$ as an effective ground state from which we apply single-photon excitation to a $^3S_1$ Rydberg state $|r\rangle$[26]. Third, instead of relying on loss through tweezer anti-trapping as in alkali systems, we employ a rapid auto-ionization scheme for Rydberg state detection. In contrast to earlier implementations of auto-ionization detection in bulk gases[21], we image remaining neutral atoms[34] instead of detecting charged particles.

More generally, our findings improve the outlook for Rydberg-based quantum computing[1–3,8–11], optimization[37] and simulation[4–7]. These applications all rely on high fidelities for preparation, detection, single-atom operations and entanglement generation, for which we briefly summarize our results: we obtain a state preparation fidelity of 0.997(1) through a combination of coherent and incoherent transfer (see Supplementary Information). The new auto-ionization scheme markedly improves the Rydberg state detection fidelity to 0.9963–0.9996 (refs. [9,12]; see Supplementary Information). We also push the limits of single and two-qubit operations in ground-to-Rydberg-state transitions[6,9,10,12]. For example, we find π-pulse fidelities of 0.9951(9) without correcting for state preparation and measurement (SPAM) and 0.9967(9) if SPAM correction is applied (see Supplementary Information). Finally, using a conservative lower-bound procedure, we observe a two-qubit entangled Bell state fidelity of $\geq$0.980(3) and >0.991(4) without and with SPAM correction, respectively. We note that all values are obtained on average and for parallel operation in arrays of 14 atoms or 10 pairs for the non-interacting or pair-interacting case, respectively.

We begin by analysing short-time Rabi oscillations between $|g\rangle$ and $|r\rangle$ (Fig. 2a) and the auto-ionization detection scheme (Fig. 2b) in an essentially non-interacting atomic configuration ((i) in Fig. 1b). To detect atoms in $|r\rangle$, we excite the core valence electron from a 5*s* level to a 5*p* level, which then rapidly auto-ionizes the Rydberg electron (inset, Fig. 2b and Supplementary Information). The ionized

[1]Division of Physics, Mathematics and Astronomy, California Institute of Technology, Pasadena, CA, USA. [2]Jet Propulsion Laboratory, California Institute of Technology, Pasadena, CA, USA. [3]Present address: Institute for Quantum Computing, University of Waterloo, Waterloo, Ontario, Canada. [4]These authors contributed equally: Ivaylo S. Madjarov, Jacob P. Covey. ✉e-mail: mendres@caltech.edu

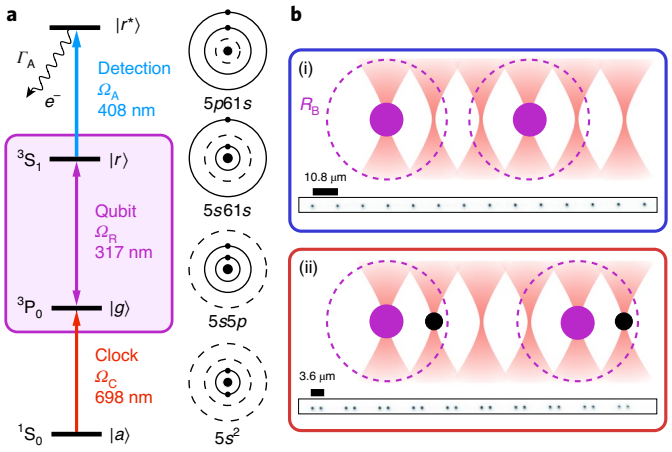

Fig. 1 | Population and detection of Rydberg states in non-interacting and interacting configurations. a, The relevant level structure (left) and electronic configuration (right) for strontium-88. The Rydberg ground-state qubit is defined by a metastable 'clock' state $|g\rangle$ and the $5s61s\ ^3S_1\ m_j=0$ Rydberg state $|r\rangle$ (highlighted with a purple box), which we detect by driving to an auto-ionizing $5p61s$ state $|r^\star\rangle$. Subscripts: A, auto-ionizing; R, Rydberg; C, clock. The clock state $|g\rangle$ is initialized from the absolute ground state $|a\rangle$. **b**, We use atom-by-atom assembly in optical tweezers to prepare an effectively non-interacting configuration ((i), blue box and blue data points throughout) and a strongly Rydberg-blockaded pair configuration ((ii), red box and red data points throughout)[7]. The blockade radius R_B, where two-atom excitation is suppressed, is indicated by a dashed circle. Throughout, purple and black circles indicate $|r\rangle$ and $|g\rangle$ atoms, respectively. The Rydberg, auto-ionization and clock beams all propagate along the axis of the atom array and address all atoms simultaneously. Averaged fluorescence images of atoms in configurations (i) and (ii) are shown. See Methods and Supplementary Information for further details.

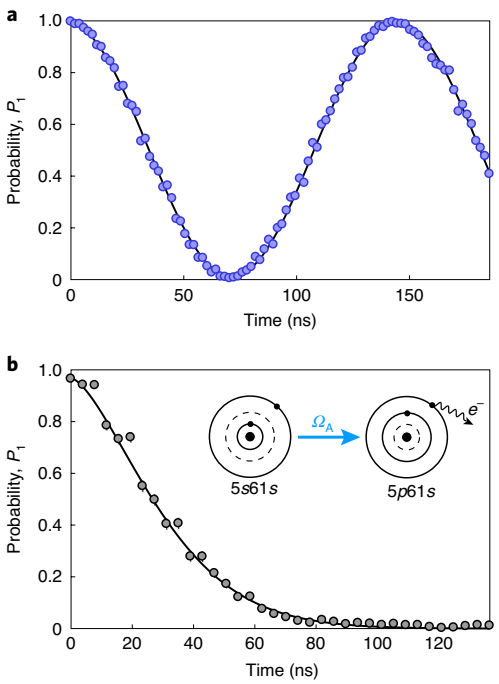

Fig. 2 | Rabi oscillations and auto-ionization. a, Array-averaged probability P_1 of detecting an atom after a resonant Rydberg pulse and subsequent auto-ionization as a function of Rydberg pulse time, showing high-contrast Rabi oscillations with frequency $\Omega_R=2\pi\times6.80(2)$ MHz. The auto-ionization pulse time is fixed to 5 μs. **b**, P_1 as a function of auto-ionization pulse time at a fixed Rydberg pulse time of 70 ns corresponding to a π-pulse (followed by a second π-pulse). The solid line is a fit to a Gaussian, phenomenologically chosen to capture the finite switch-on time of the auto-ionization beam (see Supplementary Information). Inset: illustration of the auto-ionization process. In both **a** and **b**, data are uncorrected and averaged over ~40–100 experimental cycles per time step and over an array of ~14 atoms. Error bars indicate a 1σ binomial confidence interval.

Table 1 | Uncorrected and SPAM-corrected fidelities for single-atom and Rydberg-blockaded pulses

Quantity	Uncorrected	SPAM-corrected
Single-atom π-pulse	0.9951(9)	0.9967(9)
Single-atom 2π-pulse	0.9951(9)	0.998(1)
Blockaded π-pulse	0.992(2)	0.996(2)
Blockaded 2π-pulse	0.992(2)	0.999(2)
Blockaded π-pulse, T	0.992(2)	0.996(2)
Blockaded 2π-pulse, T	0.987(2)	0.994(3)
Bell state fidelity	≥0.980(3)	≥0.991(4)
Bell state fidelity, T	≥0.975(3)	≥0.987(4)

The 'T' indicates data in which the tweezers are on during Rydberg excitation. SPAM, state preparation and measurement.

atoms are dark to subsequent detection of atoms in $|g\rangle$[34], providing the means to distinguish ground and Rydberg atoms.

We use a $|g\rangle\leftrightarrow|r\rangle$ Rabi frequency of $\Omega_R\approx2\pi\times6{-}7$ MHz throughout, and observe Rabi oscillations with high contrast at a fixed auto-ionization pulse length (Fig. 2a and Table 1). To quantify the auto-ionization detection, we perform a π-pulse on $|g\rangle\leftrightarrow|r\rangle$, then apply an auto-ionization pulse for a variable duration (Fig. 2b) and a second π-pulse on $|g\rangle\leftrightarrow|r\rangle$ before measurement. The detected population decreases to zero with a 1/e time of $\tau_A=35(1)$ ns. We can compare τ_A to the lifetime of $|r\rangle$, which is estimated to be $\tau_{|r\rangle}\approx80$ μs (ref. [38]), placing an upper bound on the $|r\rangle$-state detection efficiency of 0.9996(1). A lower bound comes from the measured π-pulse fidelity of 0.9963(9) corrected for preparation and ground-state detection errors. The upper bound can be increased with higher laser power and faster switching (see Supplementary Information).

To probe our longer time coherence, we drive the Rydberg transition for as long as 7 μs (Fig. 3a). The decay of the contrast on longer timescales is well modelled by a Gaussian profile of the form $\mathcal{C}(t)=\mathcal{C}_0\exp(-t^2/\tau_C^2)$. We find that $\tau_C\approx7$ μs is consistent with our data, and corresponds to a 1/e coherence of ~42 cycles. To our knowledge, this is the largest number of coherent ground-to-Rydberg cycles that has been published so far[9,11]. Limitations to short- and long-term coherence are discussed and modelled in detail in the Supplementary Information. The main contributing factors are laser intensity and phase noise (both can be improved with technical upgrades, such as cavity filtering of phase noise[9]), as well as the finite Rydberg-state lifetime.

We now turn to the pair-interacting configuration ((ii) in Fig. 1b) to study blockaded Rabi oscillations[1,9]. For an array spacing of 3.6 μm, we anticipate an interaction shift of $V_B\approx2\pi\times130$ MHz for the $n=61$ Rydberg state in the $^3S_1$ series[38]. In this configuration, simultaneous Rydberg excitation of closely spaced neighbours is strongly suppressed, and an oscillation between $|gg\rangle$ and the entangled W Bell state $|W\rangle=(|gr\rangle+e^{i\phi}|rg\rangle)/\sqrt{2}$ is predicted with a Rabi frequency enhanced by a factor of $\sqrt{2}$ (ref. [1]), as observed

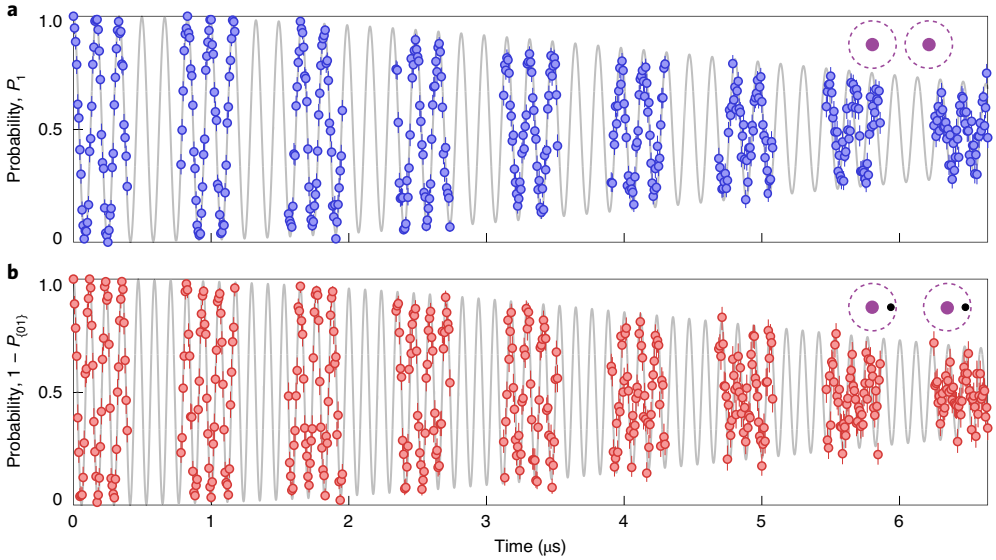

Fig. 3 | Long-time Rabi oscillations for single and blockaded atoms. a, Array-averaged Rabi oscillations for the non-interacting configuration ((i) in Fig. 1b), as depicted in the inset. We operate with $\Omega_R = 2\pi \times 6.0$ MHz. By fitting with a Gaussian profile, we find a 1/*e* coherence of ~42 cycles. **b**, Same as in **a** but for the blockaded configuration ((ii) in Fig. 1b), as depicted in the inset. We plot $1 - P_{\{01\}}$, where $P_{\{01\}}$ is the array-averaged symmetrized probability of detecting one atom of an initial pair (and not both). We observe a blockade-enhanced Rabi frequency of $\tilde{\Omega}_R = 2\pi \times 8.5$ MHz. We find a 1/*e* coherence of ~60 cycles. In both **a** and **b**, data are uncorrected and averaged over ~10 experimental cycles per time step and over an array of ~14 atoms in **a** or 10 pairs in **b**. Error bars indicate a 1σ binomial confidence interval.

in our data. We show our results for long-term coherent oscillations in Fig. 3b and find a 1/*e* coherence time corresponding to ~60 cycles. Results for short-term oscillations are shown in Fig. 4a and the fidelity values are summarized in Table 1.

We now estimate the Bell state fidelity associated with a two-atom (blockaded) π-pulse. Although parity oscillations provide a standard metric for entanglement fidelity[9], they require site-resolved laser addressing. We leave this technique for future work, and instead provide a lower bound for the Bell state fidelity based on measured populations at the (blockaded) π time and a lower bound on the purity of the two-atom state. The latter is obtained by measuring the atomic populations at the (blockaded) 2π time, under the assumption that the purity does not increase between the π and 2π times. For a detailed discussion and analysis of this bound and the validity of the underlying assumptions, see Supplementary Information. With this approach, we find uncorrected and SPAM-corrected lower bounds on the Bell state fidelity of 0.980(3) and 0.991(4), respectively (Table 1).

We note that all preceding results were obtained with the tweezers switched off during Rydberg excitation. The potential application of Rydberg gates to large-circuit-depth quantum computers motivates the study of blockade oscillations with the tweezers on. In particular, we foresee challenges for sequential gate-based platforms if tweezers must be turned off during each operation to achieve high fidelity. In systems implementing gates between the absolute ground and clock states, for example, blinking traps on and off will eventually lead to heating and loss, ultimately limiting the number of possible operations. Furthermore, while individual tweezer blinking is possible in one dimension, the prospects for blinking individual tweezers in a two-dimensional (2D) array are unclear: a 2D array generated by crossed acousto-optic deflectors cannot be blinked on the level of a single tweezer, and one generated by a spatial light modulator cannot be blinked fast enough to avoid loss. Repulsive traps such as interferometrically generated bottles[39] or repulsive lattices[10] have been developed in lieu of standard optical tweezer arrays[15,16] in part to help maintain high-fidelity operations while keeping traps on.

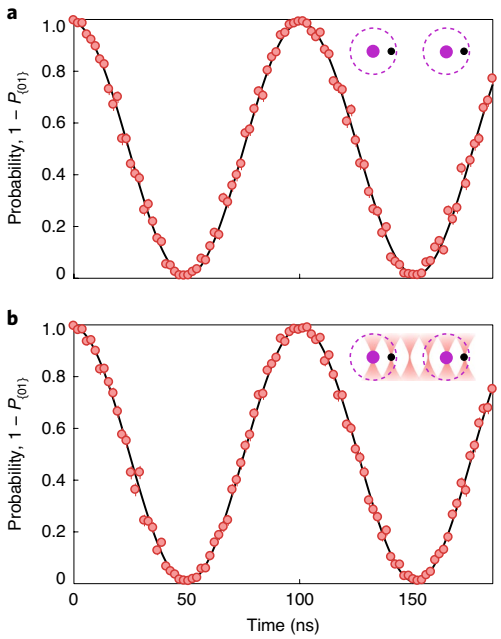

Fig. 4 | Short-time Rydberg-blockaded Rabi oscillations with tweezers off and on. a, Short-time Rabi oscillations for blockade configuration (ii) with the traps off, as depicted in the inset. **b**, Same as in **a** but with tweezers on during Rydberg interrogation with a $|g\rangle$-state depth of $U/h \approx 0.94$ MHz, where *h* is Planck's constant. The blockade-enhanced Rabi frequency is $\tilde{\Omega}_R = 2\pi \times 9.8$ MHz. In both **a** and **b**, data are uncorrected and averaged over ~50–100 experimental cycles per time step and over an array of ~10 pairs. Error bars indicate a 1σ binomial confidence interval.

Despite finding that our Rydberg state is anti-trapped (with a magnitude roughly equal to that of the ground-state trapping) at our clock magic wavelength of $\lambda_T = 813.4$ nm (see Supplementary

Information), we observe high-fidelity entanglement even when the tweezers remain on during Rydberg interrogation. Certain factors make this situation favourable for alkaline-earth atoms. One is the ability to reach lower temperatures using narrow-line cooling, which suppresses thermal dephasing due to trap light shifts. Furthermore, a lower temperature allows for ramping down of tweezers to shallower depths before atoms are lost, further alleviating dephasing. Finally, access to higher Rabi frequencies provides faster and less light-shift-sensitive entangling operations.

We study short-time blockaded Rabi oscillations both with the tweezers switched off (Fig. 4a) and left on (Fig. 4b). We find similar fidelities for the π- and 2π-pulses in both cases (Table 1). Furthermore, we estimate a lower bound for the Bell state fidelity in the tweezer on case, and find uncorrected and corrected values of $\geq$0.975(3) and $\geq$0.987(4), respectively. We expect further improvements in shorter-wavelength tweezers for which the Rydberg states of AEAs are trapped[40], and our observations show promise for Rydberg-based quantum computing in a standard tweezer array[15,16].

Our work bridges the gap between the fields of Rydberg atom arrays and optical clocks[25], opening the door to Rydberg-based quantum-enhanced metrology[26,27], including the programmable generation of spin-squeezed states[28] in recently demonstrated tweezer clocks[35,36] and quantum clock networks[29]. Furthermore, the demonstrated entangling operations provide a mechanism for two-qubit gates in AEA-based quantum computation and simulation architectures leveraging optical and nuclear qubits[30,31]. More generally, the observed entanglement fidelities could enable gate fidelities for long-lived ground states approaching fault-tolerant error-correction thresholds[41]. In addition, the high Rydberg- and ground-state detection fidelities could play an important role in applications based on sampling from bit-string probability distributions[37,42]. Finally, by auto-ionizing the Rydberg electron with high fidelity and noting that we expect the remaining ion to stay trapped, we have found a potential new approach to the optical trapping of ions[43,44] in up to 3D arrays[17,45]. Such a platform has been proposed for ion-based quantum computing[46] as well as for hybrid atom–ion systems[47–49].

Note added in proof: Recently, we became aware of work in ytterbium tweezer arrays demonstrating trapping of Rydberg states[50].

Online content

Any methods, additional references, Nature Research reporting summaries, source data, extended data, supplementary information, acknowledgements, peer review information; details of author contributions and competing interests; and statements of data and code availability are available at https://doi.org/10.1038/s41567-020-0903-z.

Received: 24 January 2020; Accepted: 7 April 2020;
Published online: 25 May 2020

References

1. Saffman, M., Walker, T. G. & Mølmer, K. Quantum information with Rydberg atoms. *Rev. Mod. Phys.* **82**, 2313–2363 (2010).
2. Browaeys, A., Barredo, D. & Lahaye, T. Experimental investigations of dipole–dipole interactions between a few Rydberg atoms. *J. Phys. B* **49**, 152001 (2016).
3. Saffman, M. Quantum computing with atomic qubits and Rydberg interactions: progress and challenges. *J. Phys. B* **49**, 202001 (2016).
4. Browaeys, A. & Lahaye, T. Many-body physics with individually controlled Rydberg atoms. *Nat. Phys.* **16**, 132–142 (2020).
5. Schauß, P. et al. Crystallization in Ising quantum magnets. *Science* **347**, 1455–1458 (2015).
6. Labuhn, H. et al. Tunable two-dimensional arrays of single Rydberg atoms for realizing quantum Ising models. *Nature* **534**, 667–670 (2016).
7. Bernien, H. et al. Probing many-body dynamics on a 51-atom quantum simulator. *Nature* **551**, 579–584 (2017).
8. Jau, Y. Y., Hankin, A. M., Keating, T., Deutsch, I. H. & Biedermann, G. W. Entangling atomic spins with a Rydberg-dressed spin-flip blockade. *Nat. Phys.* **12**, 71–74 (2016).
9. Levine, H. et al. High-fidelity control and entanglement of Rydberg-atom qubits. *Phys. Rev. Lett.* **121**, 123603 (2018).
10. Graham, T. M. et al. Rydberg-mediated entanglement in a two-dimensional neutral atom qubit array. *Phys. Rev. Lett.* **123**, 230501 (2019).
11. Levine, H. et al. Parallel implementation of high-fidelity multiqubit gates with neutral atoms. *Phys. Rev. Lett.* **123**, 170503 (2019).
12. Omran, A. et al. Generation and manipulation of Schrödinger cat states in Rydberg atom arrays. *Science* **365**, 570–574 (2019).
13. Monz, T. et al. 14-qubit entanglement: creation and coherence. *Phys. Rev. Lett.* **106**, 130506 (2011).
14. Song, C. et al. Generation of multicomponent atomic Schrödinger cat states of up to 20 qubits. *Science* **365**, 574–577 (2019).
15. Barredo, D., de Leseleuc, S., Lienhard, V., Lahaye, T. & Browaeys, A. An atom-by-atom assembler of defect-free arbitrary two-dimensional atomic arrays. *Science* **354**, 1021–1023 (2016).
16. Endres, M. et al. Atom-by-atom assembly of defect-free one-dimensional cold atom arrays. *Science* **354**, 1024–1027 (2016).
17. Kumar, A., Wu, T. Y., Giraldo, F. & Weiss, D. S. Sorting ultracold atoms in a three-dimensional optical lattice in a realization of Maxwell's demon. *Nature* **561**, 83–87 (2018).
18. de Léséleuc, S., Barredo, D., Lienhard, V., Browaeys, A. & Lahaye, T. Analysis of imperfections in the coherent optical excitation of single atoms to Rydberg states. *Phys. Rev. A* **97**, 053803 (2018).
19. DeSalvo, B. J. et al. Rydberg-blockade effects in Autler–Townes spectra of ultracold strontium. *Phys. Rev. A* **93**, 022709 (2016).
20. Gaul, C. et al. Resonant Rydberg dressing of alkaline-earth atoms via electromagnetically induced transparency. *Phys. Rev. Lett.* **116**, 243001 (2016).
21. Lochead, G., Boddy, D., Sadler, D. P., Adams, C. S. & Jones, M. P. A. Number-resolved imaging of excited-state atoms using a scanning autoionization microscope. *Phys. Rev. A* **87**, 053409 (2013).
22. Norcia, M. A., Young, A. W. & Kaufman, A. M. Microscopic control and detection of ultracold strontium in optical-tweezer arrays. *Phys. Rev. X* **8**, 041054 (2018).
23. Cooper, A. et al. Alkaline-earth atoms in optical tweezers. *Phys. Rev. X* **8**, 041055 (2018).
24. Saskin, S., Wilson, J. T., Grinkemeyer, B. & Thompson, J. D. Narrow-line cooling and imaging of ytterbium atoms in an optical tweezer array. *Phys. Rev. Lett.* **122**, 143002 (2019).
25. Ludlow, A. D., Boyd, M. M., Ye, J., Peik, E. & Schmidt, P. O. Optical atomic clocks. *Rev. Mod. Phys.* **87**, 637–701 (2015).
26. Gil, L. I. R., Mukherjee, R., Bridge, E. M., Jones, M. P. A. & Pohl, T. Spin squeezing in a Rydberg lattice clock. *Phys. Rev. Lett.* **112**, 103601 (2014).
27. Kessler, E. M. et al. Heisenberg-limited atom clocks based on entangled qubits. *Phys. Rev. Lett.* **112**, 190403 (2014).
28. Kaubruegger, R. et al. Variational spin-squeezing algorithms on programmable quantum sensors. *Phys. Rev. Lett.* **123**, 260505 (2019).
29. Kómár, P. et al. A quantum network of clocks. *Nat. Phys.* **10**, 582–587 (2014).
30. Daley, A. J., Boyd, M. M., Ye, J. & Zoller, P. Quantum computing with alkaline-earth-metal atoms. *Phys. Rev. Lett.* **101**, 170504 (2008).
31. Gorshkov, A. V. et al. Alkaline-earth-metal atoms as few-qubit quantum registers. *Phys. Rev. Lett.* **102**, 110503 (2009).
32. Kaufman, A. M. et al. Entangling two transportable neutral atoms via local spin exchange. *Nature* **527**, 208–211 (2015).
33. Welte, S., Hacker, B., Daiss, S., Ritter, S. & Rempe, G. Photon-mediated quantum gate between two neutral atoms in an optical cavity. *Phys. Rev. X* **8**, 011018 (2018).
34. Covey, J. P., Madjarov, I. S., Cooper, A. & Endres, M. 2000-times repeated imaging of strontium atoms in clock-magic tweezer arrays. *Phys. Rev. Lett.* **122**, 173201 (2019).
35. Madjarov, I. S. et al. An atomic-array optical clock with single-atom readout. *Phys. Rev. X* **9**, 041052 (2019).
36. Norcia, M. A. et al. Seconds-scale coherence on an optical clock transition in a tweezer array. *Science* **366**, 93–97 (2019).
37. Pichler, H., Wang, S. T., Zhou, L., Choi, S. & Lukin, M. D. Quantum optimization for maximum independent set using Rydberg atom arrays. Preprint at http://arxiv.org/abs/1808.10816 (2018).
38. Vaillant, C. L., Jones, M. P. A. & Potvliege, R. M. Long-range Rydberg–Rydberg interactions in calcium, strontium and ytterbium. *J. Phys. B* **45**, 135004 (2012).
39. Barredo, D. et al. Three-dimensional trapping of individual Rydberg atoms in ponderomotive bottle beam traps. *Phys. Rev. Lett.* **124**, 023201 (2020).
40. Mukherjee, R., Millen, J., Nath, R., Jones, M. P. A. & Pohl, T. Many-body physics with alkaline-earth Rydberg lattices. *J. Phys. B* **44**, 184010 (2011).
41. Knill, E. Quantum computing with realistically noisy devices. *Nature* **434**, 39–44 (2005).

42. Arute, F. et al. Quantum supremacy using a programmable superconducting processor. *Nature* **574**, 505–510 (2019).
43. Karpa, L., Bylinskii, A., Gangloff, D., Cetina, M. & Vuletić, V. Suppression of ion transport due to long-lived subwavelength localization by an optical lattice. *Phys. Rev. Lett.* **111**, 163002 (2013).
44. Huber, T., Lambrecht, A., Schmidt, J., Karpa, L. & Schaetz, T. A far-off-resonance optical trap for a Ba^+ ion. *Nat. Commun.* **5**, 5587 (2014).
45. Barredo, D., Lienhard, V., de Léséleuc, S., Lahaye, T. & Browaeys, A. Synthetic three-dimensional atomic structures assembled atom by atom. *Nature* **561**, 79–82 (2018).
46. Cirac, J. I. & Zoller, P. A scalable quantum computer with ions in an array of microtraps. *Nature* **404**, 579–581 (2000).
47. Engel, F. et al. Observation of Rydberg blockade induced by a single ion. *Phys. Rev. Lett.* **121**, 193401 (2018).
48. Mukherjee, R. Charge dynamics of a molecular ion immersed in a Rydberg-dressed atomic lattice gas. *Phys. Rev. A* **100**, 013403 (2019).
49. Langin, T. K., Gorman, G. M. & Killian, T. C. Laser cooling of ions in a neutral plasma. *Science* **363**, 61–64 (2019).
50. Wilson, J. et al. Trapped arrays of alkaline earth Rydberg atoms in optical tweezers. Preprint at http://arxiv.org/abs/1912.08754 (2019).

Methods

Here, we briefly summarize the relevant features of our ^{88}Sr experiment[23,34,35]. We used a 1D array of 43 tweezers spaced by 3.6 μm. Atoms were cooled close to the tranverse motional ground state using narrow-line cooling[34–36], with an average occupation number of $\bar{n}_r \approx 0.3$ ($T_r \approx 2.5$ μK), in tweezers of ground-state depth $U_0 \approx k_B \times 450$ μK $\approx h \times 9.4$ MHz, where k_B is Boltzmann's constant, with a radial trapping frequency of $\omega_r \approx 2\pi \times 78$ kHz.

For state preparation (Fig. 1a), we drove from the $5s^2\,{}^1S_0$ absolute ground state (labelled $|a\rangle$) to the $5s5p\,{}^3P_0$ clock state (labelled $|g\rangle$) with a narrow-line laser[35], reaching Rabi frequencies of $\Omega_C \approx 2\pi \times 3.5$ kHz in a magnetic field of ~710 G (refs. [51,52]; otherwise set to ~71 G for the entire experiment). We populated $|g\rangle$ with a π-pulse reaching a loss-corrected fidelity of 0.986(2), which we supplemented with incoherent pumping (after adiabatically ramping down the tweezer depth to $U_F = U_0/10$) to obtain a clock state population without and with loss correction of 0.997(1) and 0.998(1), respectively. This value is similar to, or higher than, the state preparation fidelities achieved with alkali atoms[10–12,53].

We treated the long-lived state $|g\rangle$ as a new ground state, from which we drove to the $5s61s\,{}^3S_1$, $m_J = 0$ Rydberg state (labelled $|r\rangle$). The $|g\rangle \leftrightarrow |r\rangle$ Rydberg transition occurred at a wavelength of $\lambda_R = 316.6$ nm and we used a $1/e^2$ beam radius of 18(1) μm. We readily achieved a $|g\rangle \leftrightarrow |r\rangle$ Rabi frequency of $\Omega_R \approx 2\pi \times 6$–$7$ MHz, corresponding to ~30 mW, and up to $\Omega_R \approx 2\pi \times 13$ MHz with full optimization of the laser system and beam path. To detect atoms in $|r\rangle$ we drove the strong transition to $5p_{3/2}61s_{1/2}$ ($J = 1$, $m_J = \pm 1$), labelled $|r'\rangle$. This transition excited the core ion, which then rapidly auto-ionized the Rydberg electron. The ionized atoms are dark to subsequent detection of atoms in $|g\rangle$ with the high-fidelity scheme described in ref. [34], providing the means to distinguish ground and Rydberg atoms. We switched off the ramped-down tweezers during the Rydberg pulse[6,7], then applied an auto-ionization pulse while rapidly increasing the depth back to U_0 for subsequent readout.

The Rydberg and clock laser beams were linearly polarized along the magnetic field axis, and the auto-ionization beam was linearly polarized perpendicular to the magnetic field axis. Accordingly, we excited to auto-ionizing states with $m_J = \pm 1$. The tweezers were linearly polarized along the axis of propagation of the Rydberg, clock and auto-ionization beams, perpendicular to the magnetic field axis.

Data availability

The data that support the findings of this study are available from the corresponding author upon reasonable request.

References

51. Taichenachev, A. et al. Magnetic field-induced spectroscopy of forbidden optical transitions with application to lattice-based optical atomic clocks. *Phys. Rev. Lett.* **96**, 083001 (2006).
52. Barber, Z. et al. Direct excitation of the forbidden clock transition in neutral ^{174}Yb atoms confined to an optical lattice. *Phys. Rev. Lett.* **96**, 083002 (2006).
53. Wang, Y., Kumar, A., Wu, T. Y. & Weiss, D. S. Single-qubit gates based on targeted phase shifts in a 3D neutral atom array. *Science* **352**, 1562–1565 (2016).

Acknowledgements

We acknowledge discussions with C. Greene and H. Levine as well as funding provided by the Institute for Quantum Information and Matter, an NSF Physics Frontiers Center grant (no. PHY-1733907), an NSF CAREER award (1753386), AFOSR YIP (FA9550-19-1-0044), the Sloan Foundation and F. Blum. Research was carried out at the Jet Propulsion Laboratory and the California Institute of Technology under a contract with the National Aeronautics and Space Administration and funded through the President's and Director's Research and Development Fund (PDRDF). J.P.C. acknowledges support from the PMA Prize postdoctoral fellowship and J.C. acknowledges support from the IQIM postdoctoral fellowship. H.P. acknowledges support by the Gordon and Betty Moore Foundation. A.K. acknowledges funding from the Larson SURF fellowship and Caltech Student-Faculty Programs.

Author contributions

M.E. conceived the idea and initiated the study. I.S.M., J.P.C., A.L.S., J.C., A.C. and V.S. designed and carried out the experiments. I.S.M., J.P.C., A.L.S., J.C., A.K. and H.P. performed theory and simulation work. I.S.M., J.P.C., A.L.S. and J.C. contributed to data analysis. I.S.M., J.P.C., A.L.S., J.C. and M.E. contributed to writing the manuscript and the Supplementary Information. J.P.C., J.R.W. and M.E. supervised and guided this work.

Competing interests

The authors declare no competing interests.

Additional information

Supplementary information is available for this paper at https://doi.org/10.1038/s41567-020-0903-z.

Correspondence and requests for materials should be addressed to M.E.

Peer review information *Nature Physics* thanks Markus Hennrich, Thierry Lahaye and Wenhui Li for their contribution to the peer review of this work.

Reprints and permissions information is available at www.nature.com/reprints.